Letter

Impact of spin-orbit splitting on two-photon absorption spectra in a halide perovskite single crystal

Keiichi Ohara,[1] Takumi Yamada,[1] Tomoko Aharen,[1] Hirokazu Tahara,[1] Hideki Hirori,[1] Hidekatsu Suzuura,[2] and Yoshihiko Kanemitsu[1,*]

[1]*Institute for Chemical Research, Kyoto University, Uji 611-0011, Japan*

[2]*Graduate School of Engineering, Hokkaido University, Sapporo 060-8628, Japan*

(Received 2 November 2020; accepted 15 December 2020; published 6 January 2021)

Metal halide perovskites have emerged as versatile photonic device materials because of their outstanding optical properties. Here, we report the two-photon absorption (TPA) spectra for $CH_3NH_3PbBr_3$ perovskite single crystals under linearly and circularly polarized laser pulses. We experimentally determined the spin-orbit splitting energy from the TPA linear-circular dichroism spectrum and found the higher-energy band around 0.8 eV above the band edge. From a theoretical analysis of the experimental data, we evaluated the exciton binding energy and the exciton reduced mass. Our findings provide essential information on the electronic structures and carrier dynamics of halide perovskites.

DOI: 10.1103/PhysRevB.103.L041201

Lead halide perovskites, described by the chemical formula $APbX_3$ (X = I, Br, Cl), are semiconductors that exhibit outstanding optoelectronic properties for device applications [1–3]. Since defect levels hardly form within the band gap, perovskite films with high enough quality to work as high-performance devices can be fabricated even in simple solution-based processes. These defect-tolerant perovskites are direct-gap semiconductors and have excellent optical properties, such as a sharp absorption edge and large absorption coefficient in the visible region, highly efficient band-edge luminescence, and exceptionally long carrier lifetime [4–8]. Thus, intensive research on optical devices, such as solar cells and light emitting diodes, has been conducted [9–12]. Perovskites have also received attention as nonlinear device materials (e.g., for two-photon excitation photoluminescence [13–15] and lasing [16,17], light modulators [18], and high harmonic generation [19,20]). Here, a deep understanding of their nonlinear optical responses is required.

Two-photon absorption (TPA) processes, which are fundamental nonlinear absorption processes, are important not only in applications but also for understanding material-specific electronic states. As can be seen in the optical selection rules of two-photon transitions, information on the electronic structure that cannot be accessed with one-photon transitions can be obtained by TPA spectroscopy [21], and thus, they can be used to investigate the electronic structures of semiconductors. However, there are only a few investigations on TPA processes in lead halide perovskites, and the reported values of the TPA coefficients are scattered over a large range [22–25]. The nonlinear optical phenomena in these perovskites are not well understood. Because of observations of novel phenomena in lead halide perovskites, such as Rashba splitting of the band edge [26,27], optically active triplet exciton [28,29], negative thermo-optic coefficient [30,31], and exceptionally slow hot-carrier relaxation [32–34], it is becoming more and more evident that the electronic structure of lead halide perovskites is different from that of conventional semiconductors. In TPA spectroscopy, it is possible to obtain detailed information by utilizing TPA anisotropy and linear-circular dichroism [35,36].

In this work, we investigated the TPA characteristics of a $CH_3NH_3PbBr_3$ single crystal in a broad energy range in order to clarify the electronic structure including the higher-energy bands, which is important for understanding hot-carrier relaxation processes. We measured the absolute values of the TPA coefficient as well as the excitation wavelength dependences of the TPA with circularly and linearly polarized light. By analyzing these results with an eight-band model based on Kanes's $\boldsymbol{k}\cdot\boldsymbol{p}$ method, we clarified the TPA dichroism and the high-energy electronic structure caused by spin-orbit splitting. From the experimental results and a theoretical analysis of the TPA spectra, we determined the spin-orbit splitting energy, exciton binding energy, and reduced exciton mass, which characterize the electronic structure of $CH_3NH_3PbBr_3$.

The $CH_3NH_3PbBr_3$ single crystal samples were fabricated by antisolvent vapor-assisted crystallization [37]. The Laue pattern of a cleaved sample measured with a back-reflection Laue method indicated a cubic phase with a (001) surface (shown in Fig. S1 of the Supplemental Material [38]). A cleaved single crystal sample with good crystallinity allows for precise measurement of the crystal-orientation dependence in the TPA spectroscopy without extrinsic factors such as light scattered from rough surfaces [24].

The TPA properties are usually examined by measuring the transmitted light intensity under strong excitation fluence. The change in intensity of light, I, that passes through the material along the optical axis z can be described by $dI/dz = -(\alpha + \beta I)I$ [39], where α is the linear absorption coefficient, and β is the TPA coefficient. If we assume that the incident pulse has a Gaussian beam profile and α is zero [39], the ratio of incident light intensity I_0 to transmitted light intensity

*Corresponding author: kanemitu@scl.kyoto-u.ac.jp

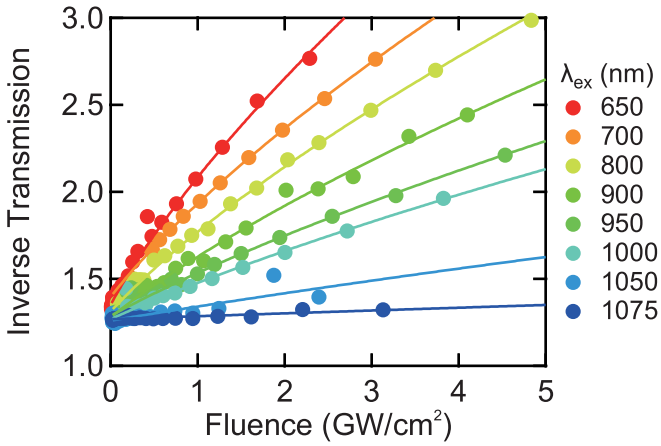

FIG. 1. Excitation fluence dependence of the inverse transmission for the $CH_3NH_3PbBr_3$ single crystal for different excitation wavelengths λ_{ex}. The solid lines are fitting results with Eq. (1).

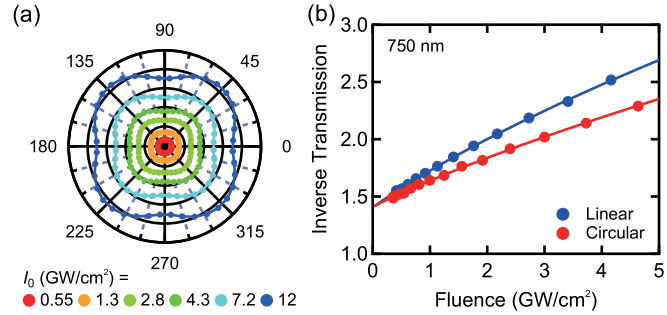

FIG. 2. (a) Dependence of transmitted light intensity at 750 nm on the polarization angle of linearly polarized light and its excitation fluence dependence. (b) Excitation fluence dependence of the inverse transmission of linear and circular polarized light at wavelength of 750 nm. The data measured under linearly and circularly polarized illumination conditions are shown in red and blue, respectively.

I_T [inverse transmission (IT)] is described by the following equation.

$$\frac{I_0}{I_T} = \frac{\sqrt{\pi}\beta I_0(1-R)L}{\int_{-\infty}^{\infty} \ln\left[1+\beta I_0(1-R)Le^{-\tau^2}\right]d\tau} \times f. \qquad (1)$$

Here, R is the reflectance at the sample surface, and the sample thickness is $L = 0.841$ mm. f is a constant that takes account of the loss in the light intensity due to factors such as surface and back-surface reflection, and it corresponds to an extrapolation to an excitation power of $0\,\mathrm{GW/cm^2}$ [14]. By employing the optical setup shown in Fig. S2(a) in the Supplemental Material [38], we measured the excitation fluence dependences of the IT. The repetition rate was 10 kHz, and the excitation fluence was adjusted by a variable neutral density filter. Moreover, the excitation wavelength was changed from 650 to 1075 nm in steps of 25 nm. By using Eq. (1), we can determine the TPA coefficient β at each wavelength.

Figure 1 shows a representative excitation fluence dependence of the IT and its change with excitation wavelength. The detailed data are shown in Fig. S2(b) in the Supplemental Material [38]. f is about 1.3 for any wavelength in the measured wavelength region. This corresponds to a reflectivity of 0.12 and agrees with the literature value for $CH_3NH_3PbBr_3$ [5]. As the excitation wavelength becomes longer, the inclination of the IT becomes smaller; it is almost zero at 1075 nm. The excitation energy corresponding to 1075 nm is almost coincident with the energy of the TPA edge of $CH_3NH_3PbBr_3$ (the band-gap energy of 2.35 eV [15]). The solid curves in Fig. 1 show the fitting results obtained using Eq. (1), and they reproduce the measurement results well. We can obtain the excitation wavelength dependence of the TPA coefficient β of $CH_3NH_3PbBr_3$ from this analysis; the results are discussed later.

The TPA coefficient reflects the electronic band structure of the material. Even in materials that belong to the cubic crystal system, anisotropic behavior and linear-circular dichroism appears in the TPA spectra [35,36]. This is because the third-order nonlinear optical susceptibility has nonzero off-diagonal elements, which is in contrast to the linear susceptibility. These nonlinear optical coefficients, such as β, are useful means of probing information on the high-energy bands or the symmetry of the band structure of a semiconductor [35,36].

Figure 2(a) shows the polarization angle dependence of the transmitted light intensity obtained for an excitation wavelength of 750 nm and by changing the excitation fluence. θ is the angle between the polarization direction of the linearly polarized light and the crystal axis [100]. As the excitation fluence increases, clear anisotropic behavior with a fourfold rotational symmetry appears in the transmitted light intensity. This fourfold rotational symmetry can be explained by the symmetry of $CH_3NH_3PbBr_3$ (space group *Pm3m*) [40]. In addition, similar anisotropic behavior appears in high harmonic generation from lead halide perovskites [20].

Figure 2(b) presents the excitation fluence dependences of the IT measured under both linearly polarized along [100] and circularly polarized excitation conditions for an excitation wavelength of 750 nm. Under both conditions, the light was normally incident on the (001) plane. From the inclinations in Fig. 2(b), we find that the TPA coefficient obtained for linearly polarized incident light, $\beta^L(\theta = 0)$, is larger than that for circularly polarized incident light, β^C. This difference is called TPA dichroism. We performed these measurements by changing the excitation wavelength from 1050 to 650 nm. The details on these data are shown in Figs. S3 and S4 in the Supplemental Material [38].

The TPA anisotropy and TPA dichroism strongly reflect the band structure of the material [35,36]. In particular, the TPA dichroism is sensitive to the higher-energy band. Thus, even if it is analyzed by a relatively simple model that accounts for the band edge and the spin split-off band, it provides important information about the electronic states, such as the spin-orbit splitting energy. Here, we focused on the excitation wavelength dependence of the TPA dichroism and analyzed the resulting spectrum.

At room temperature, $CH_3NH_3PbBr_3$ is a cubic crystal and its space group is *Pm3m* [40]. When we consider the permutation symmetry of *Pm3m* and two incident photons with equal energies, the independent nonzero tensor components of the third-order nonlinear susceptibility are only $\chi^{(3)}_{xxxx}$, $\chi^{(3)}_{xyxy}$, and $\chi^{(3)}_{xxyy}$. By employing these three tensor components, the TPA

anisotropy parameter σ and the TPA dichroism parameter δ can be defined as shown below [35,36].

$$\sigma = \frac{\chi^{(3)}_{xxxx} - \chi^{(3)}_{xxyy} - 2\chi^{(3)}_{xyyx}}{\chi^{(3)}_{xxxx}}, \tag{2}$$

$$\delta = \frac{\chi^{(3)}_{xxxx} + \chi^{(3)}_{xxyy} - 2\chi^{(3)}_{xyyx}}{2\chi^{(3)}_{xxxx}}. \tag{3}$$

Furthermore, by employing the TPA coefficients $\beta^L(\theta)$ and β^C obtained for linearly and circularly polarized light excitation, respectively, σ and δ can be expressed as follows [35,36]:

$$\sigma = \frac{2(\beta^L(0) - \beta^L(\pi/4))}{\beta^L(0)}, \tag{4}$$

$$\delta = \frac{\beta^L(0) - \beta^C}{\beta^L(0)}. \tag{5}$$

Equations (4) and (5) indicate that, by measuring $\beta^L(\theta)$ and β^C, σ and δ can be obtained experimentally. It is known that the TPA dichroism δ is sensitive to distant bands through spin-orbit splitting. In GaAs and other representative semiconductors, it has been theoretically predicted that the spin split-off band exists at the energy where the minimum of δ appears [35,36].

From an analysis of the above measurements, we determined the excitation energy (wavelength) dependence of the TPA coefficient β as well as the TPA anisotropy σ and TPA dichroism δ. The results are summarized in Fig. 3. The measured β values are plotted with the excitation energy $\hbar\omega$ on the top axis in Fig. 3(a). The figure indicates that TPA occurs at and above an excitation energy of about half of the band-gap energy of $CH_3NH_3PbBr_3$ (2.35 eV) [15]. Moreover, the increase in β is gentle up to an excitation energy of 1.6 eV, but it becomes steeper as the energy exceeds 1.6 eV. This suggests the existence of a higher-energy band. However, it is difficult to determine the precise energy of the higher band from this spectrum.

Figure 3(b) shows the excitation energy dependence of the TPA anisotropy parameter σ. Nonzero values of σ are obtained, while there is little dependence on the excitation energy. Obviously, this anisotropy reflects the cubic crystal structure of $CH_3NH_3PbBr_3$. However, the almost flat spectral shape of σ seems to be of no practical use for evaluation of the spin-orbit splitting energy in conduction bands.

The detailed electronic structures of the higher-energy bands cannot be sufficiently analyzed from β and σ, while the dichroism parameter δ can clarify their origins. Figure 3(c) presents the excitation energy dependence of the TPA dichroism parameter δ, and the local minimum of δ is around 1.6 eV. It is known that the spin split-off band exists at the energy where the minimum of δ appears [35,36]. From Figs. 3(a) and 3(c), we find that the local minimun corresponds to the energy where β again starts to increase significantly. From these results we consider that, at photon energies above 1.6 eV, there are contributions due to two-photon transitions towards the higher-energy bands, which are caused by spin-orbit splitting.

To evaluate the TPA coefficient β and the TPA dichroism δ in Fig. 3, we performed a numerical calculation using the Kane model. Lead halide perovskites are direct-gap semiconductors that have s-like valence bands and p-like conduction bands [28]. Due to the spin-orbit interaction, the six conduction-band bottom states with the spin degree of freedom are split into fourfold states with two types of

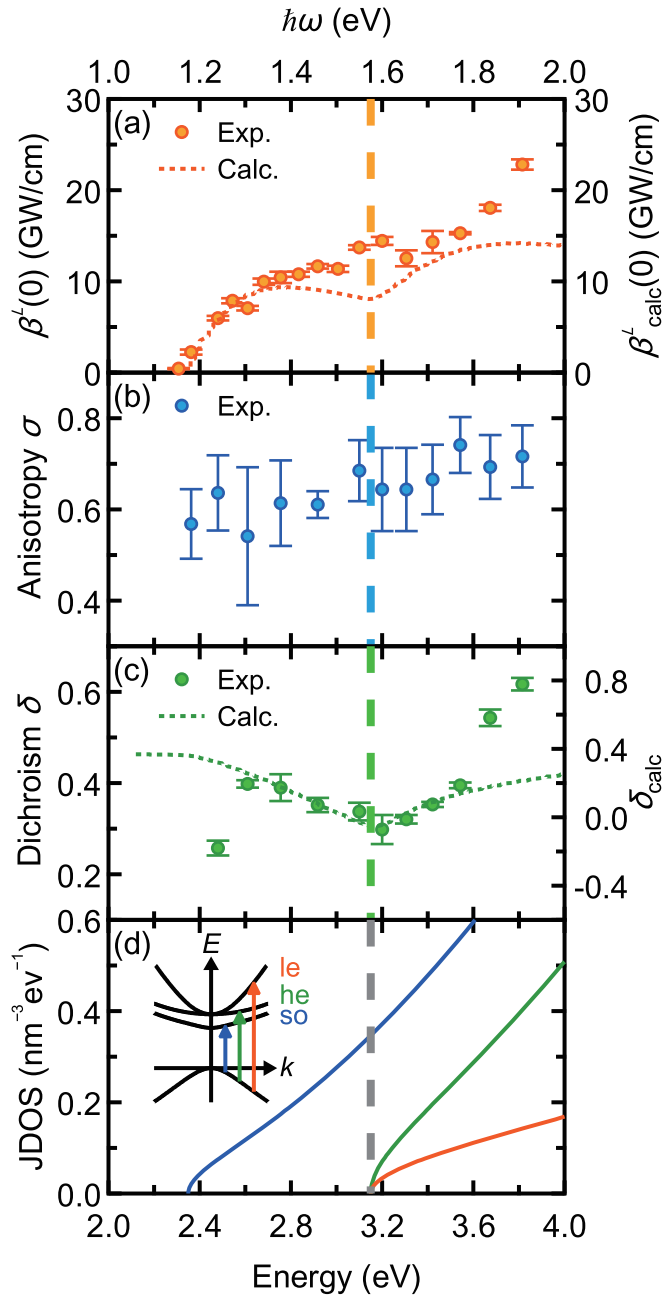

FIG. 3. Excitation energy $\hbar\omega$ (top axis) dependence of (a) two-photon absorption (TPA) coefficient β, (b) TPA anisotropy σ, and (c) TPA dichroism δ. (d) Joint density of states (JDOS) in $CH_3NH_3PbBr_3$ was calculated using the 8 × 8 Kane model. The split-off, heavy-electron, and light-electron bands are denoted by so, he, and le, respectively. The energy of the bottom axis corresponds to $2\hbar\omega$ and $E_c - E_v$. The inset shows the k-space dispersion plot of the band structure. The dotted lines in (a) and (c) are results calculated with the 8 × 8 Kane model. The vertical dashed lines in all four panels indicate the lowest energy of the heavy- and light-electron bands.

effective masses for nonzero wave vectors $\boldsymbol{k}$ and twofold ones. The latter gives the lowest conduction band and its energy decrease is equal to the spin-orbit splitting energy, as is the case with that of the spin-split-off valence band in conventional semiconductors. Thus, the band edges of the perovskite are formed by an *s*-like valence band and spin-split-off conduction band [28,41]. Since the spin-orbit splitting energy caused by Pb is large, the optical responses near the band edge of lead halide perovskites can be well explained by a 4×4 Kane model (two-band model), which only considers the band edges [24,28]. However, in analyzing TPA in a broad energy range, it is necessary to consider the higher-energy conduction bands with light and heavy effective masses. Therefore, we will consider instead an 8×8 Kane model including light- and heavy-electron bands in addition to the band edges consisting of valence and split-off bands [42]. Note that each energy band in the 8×8 Kane model shows an isotropic dispersion relation. So, other remote bands should be taken into account in order to discuss the TPA anisotropy.

The required eigenstates of $CH_3NH_3PbBr_3$ can be calculated by assuming an 8×8 Kane model and mixing the eight states including spin by $\boldsymbol{k} \cdot \boldsymbol{p}$ theory. Figure 3(d) is a plot of the calculated joint density of states (JDOS) in $CH_3NH_3PbBr_3$. The bottom axis corresponds to the energy differences between each conduction band and the valence band, $E_c - E_v$, which equals $2\hbar\omega$. Furthermore, we calculated the TPA coefficient and the TPA dichroism by using these eigenstates and second-order perturbation theory [43]. The details of the calculation are summarized in the Supplemental Material [38].

First, we discuss the results of the TPA dichroism δ. In the 8×8 Kane model, the value of δ is determined by the excitation energy $\hbar\omega$, band-gap energy E_g, and spin-orbit splitting energy Δ. Our previous work indicated that the band-gap energy of $CH_3NH_3PbBr_3$ at room temperature is 2.35 eV [15]. The spin-orbit splitting energy Δ can be determined from the local minimum of the TPA dichroism δ on the excitation energy [35,36]. The green dashed curve in Fig. 3(c) is the numerical solution for $\Delta = 0.8\,\text{eV}$, and it well reproduces the experimental characteristics; i.e., it has a local minimum near 1.6 eV. Based on the above results, we were able to determine a spin-orbit splitting energy of $\Delta = 0.8\,\text{eV}$ for $CH_3NH_3PbBr_3$. This value is very close to the value reported in Ref. [5].

Second, by using the spin-orbit splitting energy $\Delta = 0.8\,\text{eV}$, we analyze the excitation energy dependence of the TPA coefficient β. This dependence can be calculated numerically using the 8×8 Kane model [38]. We note that since the linear absorption spectrum of $CH_3NH_3PbBr_3$ has an exciton peak [5], the Coulomb interaction between an electron and a hole has to be considered. Taking the Coulomb interaction into account by using the Sommerfeld factor $C(\hbar\omega)$, the TPA coefficient for linearly polarized light excitation is given by the following equation [24,38].

$$\beta(\hbar\omega) = \frac{K}{n_0^2 E_g^3}\sqrt{\frac{3m_0 E_g}{2\mu\left(1+\frac{E_g}{E_g+\Delta}\right)}}\,C(\hbar\omega)F_\Delta(\hbar\omega). \quad (6)$$

Here, K is a constant that reflects the character of the band-to-band transition matrix elements. A theoretical value of $K = 1867$ has been obtained for lead halide perovskites [24]. The linear refractive index n_0 of $CH_3NH_3PbBr_3$ has an almost constant value of 2.05 in this wavelength region [5]. The Sommerfeld factor is defined by $C(\hbar\omega) = xe^x/\sinh x$, where $x = \pi\sqrt{E_b/(2\hbar\omega - E_g)}$. E_b is the exciton binding energy, and μ is the reduced exciton mass. $F_\Delta(\hbar\omega)$ is a dimensionless function that determines the wavelength dependence, and it can be obtained from a numerical calculation [38].

In order to evaluate the exciton binding energy E_b and reduced exciton mass μ in the lowest band, we fitted the experimental data of the TPA coefficient β using Eq. (6) below 1.5 eV. The result is shown as the orange dashed curve in Fig. 3(a). For the fitting parameters, we obtained an exciton binding energy E_b of 28 meV and a reduced exciton mass μ of $0.089m_0$. Similar values have been obtained by magneto-optical spectroscopy at low temperatures [44,45]. Note that the effects of band nonparabolicity or excitons at higher states are considered to be the reason for the deviation from the experimental data in the high-energy region. On the other hand, the band edge structure of β can be accurately reproduced by our model. We successfully determined the spin-orbit splitting energy, exciton binding energy, and reduced mass using a model that includes the light- and heavy-electron bands and the Coulomb interaction.

In conclusion, we studied the excitation energy dependences of the TPA coefficient, TPA anisotropy, and TPA dichroism of $CH_3NH_3PbBr_3$. From the TPA dichroism spectrum, we experimentally determined that the spin-orbit splitting energy is approximately 0.8 eV. By numerically analyzing the measured data using an 8×8 Kane model and considering the role of the Coulomb interaction on the TPA spectra, we evaluated the exciton binding energy and the reduced mass. Our findings provide a direct experimental reference on the electronic structure of halide perovskites for optoelectronic applications.

The authors thank Dr. T. Kikuchi of Rigaku Corporation for the x-ray Laue measurements. Part of this work was supported by JSPS KAKENHI (JP19H05465 and JP20K03798) and CREST, JST (JPMJCR16N3).

[1] S. D. Stranks and H. J. Snaith, Metal-halide perovskites for photovoltaic and light-emitting devices, Nat. Nanotechnol. **10**, 391 (2015).

[2] B. R. Sutherland and E. H. Sargent, Perovskite photonic sources, Nat. Photonics **10**, 295 (2016).

[3] Y. Kanemitsu, Luminescence spectroscopy of lead-halide perovskites: Materials properties and application as photovoltaic devices, J. Mater. Chem. C **5**, 3427 (2017).

[4] Q. A. Akkerman, G. Rainò, M. V. Kovalenko, and L. Manna, Genesis, challenges and opportunities for colloidal lead halide perovskite nanocrystals, Nat. Mater. **17**, 394 (2018).

[5] A. M. A. Leguy, P. Azarhoosh, M. I. Alonso, M. Campoy-Quiles, O. J. Weber, J. Yao, D. Bryant, M. T. Weller, J. Nelson, A. Walsh, M. Van Schilfgaarde, and P. R. F. Barnes, Experimental and theoretical optical properties of methylammonium lead halide perovskites, Nanoscale **8**, 6317 (2016).

[6] Y. Yamada, T. Nakamura, M. Endo, A. Wakamiya, and Y. Kanemitsu, Photocarrier recombination dynamics in perovskite $CH_3NH_3PbI_3$ for solar cell applications, J. Am. Chem. Soc. **136**, 11610 (2014).

[7] S. D. Stranks, G. E. Eperon, G. Grancini, C. Menelaou, M. J. P. Alcocer, T. Leijtens, L. M. Herz, A. Petrozza, and H. J. Snaith, Electron-hole diffusion lengths exceeding 1 micrometer in an organometal trihalide perovskite absorber, Science **342**, 341 (2013).

[8] G. Xing, N. Mathews, S. Sun, S. S. Lim, Y. M. Lam, M. Grätzel, S. Mhaisalkar, and T. C. Sum, Long-range balanced electron and hole-transport lengths in organic-inorganic $CH_3NH_3PbI_3$, Science **342**, 344 (2013).

[9] M. M. Lee, J. Teuscher, T. Miyasaka, T. N. Murakami, and H. J. Snaith, Efficient hybrid solar cells based on meso-superstructured organometal halide perovskites, Science **338**, 643 (2012).

[10] Z.-K. Tan, R. S. Moghaddam, M. L. Lai, P. Docampo, R. Higler, F. Deschler, M. Price, A. Sadhanala, L. M. Pazos, D. Credgington, F. Hanusch, T. Bein, H. J. Snaith, and R. H. Friend, Bright light-emitting diodes based on organometal halide perovskite, Nat. Nanotechnol. **9**, 687 (2014).

[11] G. Xing, N. Mathews, S. S. Lim, N. Yantara, X. Liu, D. Sabba, M. Grätzel, S. Mhaisalkar, and T. C. Sum, Low-temperature solution-processed wavelength-tunable perovskites for lasing, Nat. Mater. **13**, 476 (2014).

[12] H. Zhu, Y. Fu, F. Meng, X. Wu, Z. Gong, Q. Ding, M. V. Gustafsson, M. T. Trinh, S. Jin, and X-Y. Zhu, Lead halide perovskite nanowire lasers with low lasing thresholds and high quality factors, Nat. Mater. **14**, 636 (2015).

[13] Y. Yamada, T. Yamada, L. Q. Phuong, N. Maruyama, H. Nishimura, A. Wakamiya, Y. Murata, and Y. Kanemitsu, Dynamic optical properties of $CH_3NH_3PbI_3$ single crystals as revealed by one- and two-photon excited photoluminescence measurements, J. Am. Chem. Soc. **137**, 10456 (2015).

[14] G. Walters, B. R. Sutherland, S. Hoogland, D. Shi, R. Comin, D. P. Sellan, O. M. Bakr, and E. H. Sargent, Two-photon absorption in organometallic bromide perovskites, ACS Nano **9**, 9340 (2015).

[15] T. Yamada, Y. Yamada, H. Nishimura, Y. Nakaike, A. Wakamiya, Y. Murata, and Y. Kanemitsu, Fast free-carrier diffusion in $CH_3NH_3PbBr_3$ single crystals revealed by time-resolved one- and two-photon excitation photoluminescence spectroscopy, Adv. Electron. Mater. **2**, 1500290 (2016).

[16] Y. Xu, Q. Chen, C. Zhang, R. Wang, H. Wu, X. Zhang, G. Xing, W. W. Yu, X. Wang, Y. Zhang, and M. Xiao, Two-photon-pumped perovskite semiconductor nanocrystal lasers, J. Am. Chem. Soc. **138**, 3761 (2016).

[17] Y. Wang, X. Li, X. Zhao, L. Xiao, H. Zeng, and H. Sun, Nonlinear absorption and low-threshold multiphoton pumped stimulated emission from all-inorganic perovskite nanocrystals, Nano Lett. **16**, 448 (2016).

[18] H. Tahara, T. Aharen, A. Wakamiya, and Y. Kanemitsu, Photorefractive effect in organic–inorganic hybrid perovskites and its application to optical phase shifter, Adv. Opt. Mater. **6**, 1701366 (2018).

[19] H. Hirori, P. Xia, Y. Shinohara, T. Otobe, Y. Sanari, H. Tahara, N. Ishii, J. Itatani, K. L. Ishikawa, T. Aharen, M. Ozaki, A. Wakamiya, and Y. Kanemitsu, High-order harmonic generation from hybrid organic–inorganic perovskite thin films, APL Mater. **7**, 041107 (2019).

[20] Y. Sanari, H. Hirori, T. Aharen, H. Tahara, Y. Shinohara, K. L. Ishikawa, T. Otobe, P. Xia, N. Ishii, J. Itatani, S. A. Sato, and Y. Kanemitsu, Role of virtual band population for high harmonic generation in solids, Phys. Rev. B **102**, 041125(R) (2020).

[21] R. W. Boyd, *Nonlinear optics*, 3rd ed. (Academic, New York, 2008).

[22] A. Ferrando, J. P. Martínez Pastor, and I. Suárez, Toward metal halide perovskite nonlinear photonics, J. Phys. Chem. Lett. **9**, 5612 (2018).

[23] T. Yamada, T. Aharen, and Y. Kanemitsu, Near-Band-Edge Optical Responses of $CH_3NH_3PbCl_3$ Single Crystals: Photon Recycling of Excitonic Luminescence, Phys. Rev. Lett. **120**, 057404 (2018).

[24] K. Ohara, T. Yamada, H. Tahara, T. Aharen, H. Hirori, H. Suzuura, and Y. Kanemitsu, Excitonic enhancement of optical nonlinearities in perovskite $CH_3NH_3PbCl_3$ single crystals, Phys. Rev. Mater. **3**, 111601(R) (2019).

[25] Z. Wei, D. Guo, J. Thieme, C. Katan, V. M. Caselli, J. Even, and T. J. Savenije, The importance of relativistic effects on two-photon absorption spectra in metal halide perovskites, Nat. Commun. **10**, 5342 (2019).

[26] D. Niesner, M. Hauck, S. Shrestha, I. Levchuk, G. J. Matt, A. Osvet, and T. Fauster, Structural fluctuations cause spin-split states in tetragonal $(CH_3NH_3)PbI_3$ as evidenced by the circular photogalvanic effect, Proc. Natl. Acad. Sci. USA **115**, 9509 (2018).

[27] M. Isarov, L. Z. Tan, M. I. Bodnarchuk, M. V. Kovalenko, A. M. Rappe, and E. Lifshitz, Rashba effect in a single colloidal $CsPbBr_3$ perovskite nanocrystal detected by magneto-optical measurements, Nano Lett.**17**, 5020 (2017).

[28] M. A. Becker, R. Vaxenburg, G. Nedelcu, P. C. Sercel, A. Shabaev, M. J. Mehl, J. G. Michopoulos, S. G. Lambrakos, N. Bernstein, J. L. Lyons, T. Stöferle, R. F. Mahrt, M. V. Kovalenko, D. J. Norris, G. Rainò, and A. L. Efros, Bright triplet excitons in cesium lead halide perovskites, Nature (London) **553**, 189 (2018).

[29] P. Tamarat, M. I. Bodnarchuk, J.-B. Trebbia, R. Erni, M. V. Kovalenko, J. Even, and B. Lounis, The ground exciton state of formamidinium lead bromide perovskite nanocrystals is a singlet dark state, Nat. Mater. **18**, 717 (2019).

[30] T. Handa, H. Tahara, T. Aharen, and Y. Kanemitsu, Large negative thermo-optic coefficients of a lead halide perovskite, Sci. Adv. **5**, eaax0786 (2019).

[31] T. Handa, H. Tahara, T. Aharen, A. Shimazaki, A. Wakamiya, and Y. Kanemitsu, Large thermal expansion leads to negative thermo-optic coefficient of halide perovskite $CH_3NH_3PbCl_3$, Phys. Rev. Mater. **4**, 074604 (2020).

[32] H. Zhu, K. Miyata, Y. Fu, J. Wang, P. P. Joshi, D. Niesner, K. W. Williams, S. Jin, and X.-Y. Zhu, Screening in crystalline liquids protects energetic carriers in hybrid perovskites, Science **353**, 1409 (2016).

[33] Y. Yang, D. P. Ostrowski, R. M. France, K. Zhu, J. van de Lagemaat, J. M. Luther, and M. C. Beard, Observation of a hot-

phonon bottleneck in lead-iodide perovskites, Nat. Photonics **10**, 53 (2016).

[34] J. Chen, M. E. Messing, K. Zheng, and T. Pullerits, Cation-dependent hot carrier cooling in halide perovskite nanocrystals, J. Am. Chem. Soc. **141**, 3532 (2019).

[35] D. C. Hutchings and B. S. Wherrett, Theory of anisotropy of two-photon absorption in zinc-blende semiconductors, Phys. Rev. B **49**, 2418 (1994).

[36] D. C. Hutchings and B. S. Wherrett, Linear/circular dichroism of two-photon absorption in zinc-blende semiconductors, Opt. Mater. **3**, 53 (1994).

[37] D. Shi, V. Adinolfi, R. Comin, M. Yuan, E. Alarousu, A. Buin, Y. Chen, S. Hoogland, A. Rothenberger, K. Katsiev, Y. Losovyj, X. Zhang, P. A. Dowben, O. F. Mohammed, E. H. Sargent, and O. M. Bakr, Low trap-state density and long carrier diffusion in organolead trihalide perovskite single crystals, Science **347**, 519 (2015).

[38] See Supplemental Material at http://link.aps.org/supplemental/10.1103/PhysRevB.103.L041201 for single crystal fabrication and x-ray Laue spectroscopy, experimental setup for two-photon absorption spectroscopy, two-photon absorption with different polarization angle of linearly polarized light, two-photon absorption with linearly and circularly polarized light, derivation of exciton reduced masses for 8×8 Kane model, and derivation of excitation-photon-energy dependence and TPA dichroism for 8×8 Kane model.

[39] M. Sheik-Bahae, A. A. Said, T.-H. Wei, D. J. Hagan, and E. W. Van Stryland, Sensitive measurement of optical nonlinearities using a single beam, IEEE J. Quantum Electron. **26**, 760 (1990).

[40] F. O. Saouma, D. Y. Park, S. H. Kim, M. S. Jeong, and J. I. Jang, Multiphoton absorption coefficients of organic–inorganic lead halide perovskites $CH_3NH_3PbX_3$ (X = Cl, Br, I) single crystals, Chem. Mater. **29**, 6876 (2017).

[41] J. Even, L. Pedesseau, J. M. Jancu, and C. Katan, Importance of spin–orbit coupling in hybrid organic/inorganic perovskites for photovoltaic applications, J. Phys. Chem. Lett. **4**, 2999 (2013).

[42] P. Y. Yu and M. Cardona, *Fundamentals of Semiconductors: Physics and Materials Properties* (Springer, Berlin, 2001).

[43] C. R. Pidgeon, B. S. Wherrett, A. M. Johnston, J. Dempsey, and A. Miller, Two-Photon Absorption in Zinc-Blende Semiconductors, Phys. Rev. Lett. **42**, 1785 (1979).

[44] K. Galkowski, A. Mitioglu, A. Miyata, P. Plochocka, O. Portugall, G. E. Eperon, J. T. W. Wang, T. Stergiopoulos, S. D. Stranks, H. J. Snaith, and R. J. Nicholas, Determination of the exciton binding energy and effective masses for methylammonium and formamidinium lead tri-halide perovskite semiconductors, Energy Environ. Sci. **9**, 962 (2016).

[45] Y. Yamada, H. Mino, T. Kawahara, K. Oto, H. Suzuura, and Y. Kanemitsu, Polaron Masses in $CH_3NH_3PbX_3$ Perovskites Determined by Landau Level Spectroscopy in Low Magnetic Fields, arXiv:2001.07901.